J Biomol NMR (2009) 43:21–30
DOI 10.1007/s10858-008-9285-8

ARTICLE

Identification of HN-methyl NOEs in large proteins using simultaneous amide-methyl TROSY-based detection

Chenyun Guo · Vitali Tugarinov

Received: 25 August 2008 / Accepted: 14 October 2008 / Published online: 11 November 2008

Abstract A pair of HN-methyl NOESY experiments that are based on simultaneous TROSY-type detection of amide and methyl groups is described. The preservation of cross-peak symmetry in the simultaneous ^{1}H–^{15}N/$^{13}CH_3$ NOE spectra enables straightforward assignments of HN-methyl NOE cross-peaks in large and complex protein structures. The pulse schemes are designed to preserve the slowly decaying components of both ^{1}H–^{15}N and methyl $^{13}CH_3$ spin-systems in the course of indirect evolution (t_2) and acquisition period (t_3) of 3D NOESY experiments. The methodology has been tested on {U-[^{15}N,^{2}H]; Ileδ1-[$^{13}CH_3$]; Leu,Val-[$^{13}CH_3$,$^{12}CD_3$]}-labeled 82-kDa enzyme Malate Synthase G (MSG). A straightforward procedure that utilizes the symmetry of NOE cross-peaks in the time-shared 3D NOE data sets allows unambiguous assignments of more than 300 HN-methyl interactions in MSG from a single 3D data set providing important structural restraints for derivation of the backbone global fold.

Keywords NOE · Large proteins · TROSY · Time-shared · Methyl

Abbreviations

TROSY	Transverse relaxation optimized spectroscopy
NOE	Nuclear Overhauser effect
NOESY	NOE spectroscopy
HMQC	Heteronuclear multiple quantum correlation spectroscopy
HSQC	Heteronuclear single quantum correlation spectroscopy
MSG	Malate synthase G
PEP	Preservation of equivalent pathways
ILV	Isoleucine, leucine, valine
DTT	Dithiothreitol

C. Guo · V. Tugarinov (✉)
Department of Chemistry and Biochemistry, University of Maryland, College Park, MD 20742, USA
e-mail: vitali@umd.edu

Introduction

'Ab initio' determination of protein structures by solution NMR techniques relies upon the ability to detect a 'critical mass' of inter-proton NOEs that serve as a principal source of distance restraints in structure calculations (Wüthrich 1986). In complex high-molecular-weight systems, the measurement and assignment of all inter-proton NOEs in a protein molecule is hardly feasible due to severe resonance overlap and fast relaxation of proton signals. Therefore, approaches that utilize selective protonation and ^{13}C-labeling of only a subset of sites in a large protein while the rest of the molecule remains deuterated, are becoming increasingly popular. Because of their favorable relaxation properties, methyls are frequently positions of choice for selective ^{1}H/^{13}C incorporation (Rosen et al. 1996; Gardner et al. 1997). Robust methyl isotope labeling strategies developed by Kay and co-workers, allow selective protonation of Ile(δ1), Leuδ and Valγ (ILV) sites in otherwise deuterated proteins through the use of appropriate α-keto-acids as biosynthetic precursors in minimal D_2O-based media (Gardner and Kay 1997; Gardner et al. 1998; Goto et al. 1999; Tugarinov and Kay 2004, 2005). This labeling methodology has been successfully applied to derive the NMR-based global backbone fold of the largest monomeric protein studied by solution NMR, an 82-kDa 723-residue enzyme Malate Synthase G (MSG) (Tugarinov et al. 2005; Tugarinov and Kay 2005).

The reduction in the number of protons associated with selective ILV protonation/labeling and the concomitant decrease in the number of available distance restraints for structure generation, make it especially important to maximize the number of identifiable NOEs in the ILV-labeled protein samples. In the case of MSG, the NOEs involving methyl signals represent by far the dominant source of information for NMR-based structure derivation; 84.2% of all long-range distance restraints used in the calculations of the global fold of MSG involve methyl groups (Tugarinov and Kay 2005). Among NOEs involving ILV methyls, HN-methyl contacts are of special importance as one of the partners is a backbone atom, an important consideration in the derivation of backbone folds. 4D NOE spectroscopy has been employed for identification and assignment of the majority of NOEs used in MSG backbone fold calculations (Tugarinov et al. 2005). However, the total number of HN-methyl contacts that could be identified in the 4D $^{1}H_{m}$–$^{13}C_{m}$–^{15}N–^{1}HN HMQC–NOESY–TROSY (Muhandiram et al. 1993; Pervushin et al. 1997) spectrum of MSG was surprisingly low. Only 57 HN-methyl restraints (i.e. 7.3% of the total final number of distance restraints involving methyl groups in MSG) and among those 11 long-range ($|i - j| > 3$) NOEs (2.1% of the total final number of long-range methyl NOEs) could be obtained from this 4D data set. Inherently low sensitivity of the 4D HMQC–NOESY–TROSY data necessitated the acquisition of a pair of more sensitive 3D $^{1}H_{m}$–($^{13}C_{m}$)–^{15}N–^{1}HN and ($^{1}H_{m}$)–$^{13}C_{m}$–^{15}N–^{1}HN HMQC–NOESY–TROSY experiments. These 3D spectra lack the symmetry of NOE cross-peaks frequently leading to ambiguities in NOE assignments in such complex protein structures as MSG where a single amide may provide cross-peaks to several methyl positions. Here, we present a pair of HN-methyl NOESY experiments that are based on simultaneous TROSY-type detection (Pervushin et al. 1997) of amide and methyl groups recently developed in our group (Guo et al. 2008). The preservation of cross-peak symmetry in the simultaneous ^{1}H–^{15}N/$^{13}CH_3$ NOESY spectra enables straightforward assignments of HN-methyl NOE cross-peaks even in large and complex protein structures. The pulse schemes are designed to preserve the slowly decaying components of both ^{1}H–^{15}N and methyl $^{13}CH_3$ spin-systems in the course of indirect evolution (t_2) and acquisition period (t_3) of 3D experiments making them suitable for structural studies of proteins within at least 100-kDa molecular weight range.

Materials and methods

NMR sample

A sample of {U-[^{15}N,^{2}H]; Ileδ1-[$^{13}CH_3$]; Leu,Val-[$^{13}CH_3$,$^{12}CD_3$]}-labeled MSG was prepared in D_2O-based minimal medium as described in detail previously (Tugarinov et al. 2002, 2005; Tugarinov and Kay 2004) using U-[^{2}H]-D-glucose as the main carbon source, ^{15}N-ammonium chloride as the main source of nitrogen and appropriate α-keto-acid precursors for selective methyl labeling (Tugarinov and Kay 2005). The 0.9 mM protein sample was dissolved in 90% H_2O/10% D_2O and contained 25 mM sodium phosphate (pH 7.1), 0.05% NaN_3, 5 mM DTT, 20 mM $MgCl_2$. Of note, although the Methyl-TROSY effect (Ollerenshaw et al. 2003; Tugarinov et al. 2003) is maximized when methyl NMR spectra are recorded on samples dissolved in D_2O, H_2O had to be used in this work to make simultaneous detection of ^{1}H–^{15}N amides possible.

NMR spectroscopy

All NMR spectra were recorded on a 600 MHz (^{1}H frequency) Bruker Avance III spectrometer equipped with a room-temperature triple-resonance probe-head operating at 37°C. The 3D SIM-$^{1}H_{m}$/^{1}HN-NOESY-$^{13}C_{m}$–$^{1}H_{m}$/^{15}N–^{1}HN TROSY experiment has been recorded with 16 scans/fid and (64, 64, 512) complex points in (t_1, t_2, t_3) corresponding to acquisition times of (22, 35, 64 ms). Relaxation delay of 1.2 s led to a total experimental time of 4.3 days. Spectral widths (SW) in F_1(^{1}H) and F_2(^{15}N/$^{13}C_{m}$) dimensions correspond to 5 and 30/12 ppm, respectively. The 3D SIM-$^{13}C_{m}$/^{15}N-NOESY-$^{13}C_{m}$–$^{1}H_{m}$/^{15}N–^{1}HN TROSY experiment has been recorded with 24 scans/fid and (40, 64, 512) complex points in (t_1, t_2, t_3) corresponding to acquisition times of (22, 35, 64 ms). Relaxation delay of 1.2 s led to a total experimental time of 4.3 days. SW in F_1(^{15}N/$^{13}C_{m}$) and F_2(^{15}N/$^{13}C_{m}$) dimensions was 30/12 ppm. NOE mixing time of 190 ms was used in both experiments.

All NMR spectra were processed with the NMRPipe/NMRDraw suite of programs (Delaglio et al. 1995). Each 3D data set has been separated onto two sub-spectra: (1) downfield, and (2) upfield of the water resonance in the acquisition (F_3, ^{1}HN) dimension. This separation allows convenient labeling of the time-shared dimension (F_2) in the separated spectra with ^{15}N or ^{13}C chemical shifts. The frequency-domain data of the 3D SIM-$^{1}H_{m}$/^{1}HN-NOESY-$^{13}C_{m}$–$^{1}H_{m}$/^{15}N–^{1}HN TROSY experiment have been circular-shifted down-field by 4.2 ppm in the F_1($^{1}H_{m}$/^{1}HN) dimension ensuring double-aliasing ($+2 \times SW_{F1}$) of all diagonal methyl peaks. All isoleucine δ1 methyl signals are aliased in the F_2($^{13}C_{m}$) dimension of the 3D SIM-$^{1}H_{m}$/^{1}HN-NOESY-$^{13}C_{m}$–$^{1}H_{m}$/^{15}N–^{1}HN TROSY data set, and in both F_1($^{13}C_{m}$) and F_2($^{13}C_{m}$) dimensions of the 3D SIM-$^{13}C_{m}$/^{15}N-NOESY-$^{13}C_{m}$–$^{1}H_{m}$/^{15}N–^{1}HN TROSY data set. The spectra have been analyzed with the program NMRView (Johnson and Blevins 1994) using Tcl/Tk scripts written in house.

Results and discussion

The gradient enhanced PEP-HMQC scheme for methyl groups in large proteins

Although the concept of time-sharing in NMR experiments originally proposed by Sørensen (1990) and Farmer (1991), has been widely utilized in protein NMR (Boelens et al. 1994; Sattler et al. 1995; Würtz et al. 2007) and applied to NOE spectroscopy in a number of earlier studies (Farmer and Mueller 1994; Pascal et al. 1994; Uhrín et al. 2000; Xia et al. 2003; Frueh et al. 2006; Xu et al. 2007), none of available implementations of $^{15}N/^{13}C$ time-sharing preserves the slowly relaxing components of both $^{15}N–^{1}H$ and $^{13}CH_3$ spin-systems simultaneously in a TROSY-based manner in the course of indirect evolution and acquisition periods. The implementation of a 2D Methyl-TROSY (Methyl-HMQC) experiment (Ollerenshaw et al. 2003; Tugarinov et al. 2003) that ensures preservation of equivalent pathways (PEP) (Kay et al. 1992; Palmer et al. 1991; Schleucher et al. 1994) on the one hand, and allows preservation of the slowly relaxing magnetization in $^{13}CH_3$ spin-systems during both t_1 and t_2 evolution periods on the other hand, is germane to simultaneous $^{15}N–^{1}H/^{13}CH_3$ time-shared TROSY-based experiments (Guo et al. 2008). Therefore, we start by providing a brief description of the gradient-selected PEP-HMQC (Bax et al. 1983; Mueller 1979) pulse scheme for methyl groups (Fig. 1a) using single-transition operators. Figure 1b shows an energy level diagram and the corresponding ^{1}H transitions of interest for an isolated methyl group. For simplicity, although a $^{13}CH_3$ methyl group is considered, the '^{13}C contributions' to the energy level diagram have been omitted from the figure. In the macromolecular limit and under the assumption of very rapid rotation about the methyl three-fold axis the relaxation of each of the single quantum ^{1}H coherences, denoted by the vertical lines in Fig. 1b, occurs in a single-exponential manner with fast ($R^{F}_{2,H}$; blue arrows) or slow ($R^{S}_{2,H}$; red arrows) rates (Kay and Prestegard 1987; Tugarinov et al. 2003).

The element of this pulse-scheme enclosed in dashed rectangle in Fig. 1a achieves the TROSY-like magnetization transfer in $^{13}CH_3$ groups as follows. Considering only the first step of the phase-cycle and neglecting pulsed field gradients and relaxation for the moment, at time-point *a* of the scheme (following the t_1 period; Fig. 1a) the density operators of the two orthogonal components of the slowly relaxing part of $^{13}CH_3$ magnetization, σ^S_Y and σ^S_X, are given by,

$$\sigma^S_{Y,a} = 2C_Y\left(|2\rangle\langle3| + |3\rangle\langle2| + \frac{1}{2}|5\rangle\langle6| + \frac{1}{2}|6\rangle\langle5| + \frac{1}{2}|7\rangle\langle8| + \frac{1}{2}|8\rangle\langle7|\right)\cos(\omega_C t_1) \quad (1)$$

and

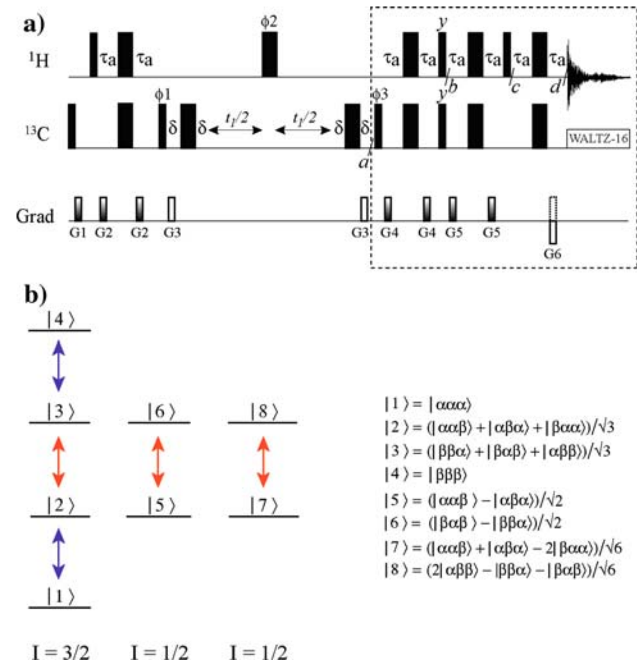

Fig. 1 **a** Pulse scheme for gradient-enhanced preservation of equivalent pathways (PEP) in $^{13}CH_3$ methyls of large proteins. All narrow (wide) rectangular pulses are applied with flip angles of 90(180)° along the *x*-axis unless indicated otherwise. All ^{1}H and ^{13}C pulses are applied with the highest possible power; ^{13}C WALTZ-16 (Shaka et al. 1983) decoupling is achieved using a 2-kHz field. Delays are: τ_a = 2.0 ms; δ = 500 µs. The durations and strengths of pulsed-field gradients in units of (ms; G/cm) are: G1 = (1; 15), G2 = (0.3; 10), G3 = (0.4; 20), G4 = (0.25; 15), G5 = (0.3; 12), G6 = (0.4; −10). Phase cycle: $\phi1 = x,-x$; $\phi2 = 2(x),2(-x)$; $\phi3 = x$; rec. = $x,-x$. Quadrature detection in t_1 is achieved via a gradient enhanced sensitivity scheme: for each t_1 value a pair of spectra is recorded with $\phi3 = x$; G_6 and $\phi3 = -x$; $-G_6$ and manipulated post-acquisition (Kay et al. 1992; Schleucher et al. 1994). The phase $\phi1$ is inverted for each t_1 point (Marion et al. 1989). **b** Energy level diagram for the (^{13}C)H_3 spin-system of a methyl group. Slow (fast) relaxing single-quantum ^{1}H transitions are shown with red(blue) arrows. The eight ^{1}H eigenstates are depicted by |i,j,k > (i,j,k ∈ {α,β}). The spin quantum numbers, I, of the three manifolds are labeled on the diagram

$$\sigma^S_{X,a} = -2C_X\left(|2\rangle\langle3| + |3\rangle\langle2| + \frac{1}{2}|5\rangle\langle6| + \frac{1}{2}|6\rangle\langle5| + \frac{1}{2}|7\rangle\langle8| + \frac{1}{2}|8\rangle\langle7|\right)\sin(\omega_C t_1) \quad (2)$$

In Eqs. 1 and 2 C_Q is the $Q \in \{X,Y,Z\}$ component of *C* spin angular momentum and operators are written in terms of individual transitions, with the eigenfunctions |j> defined as in Fig. 1b. After the ^{13}C pulse ($\phi3$) and the subsequent $2\tau_a$ period followed by a pair of $^{1}H_y/^{13}C_y$ pulses (time point *b* in Fig. 1a), the two orthogonal components of the slow-relaxing part will transform to,

$$\sigma^S_{Y,b} = \begin{pmatrix} \frac{\sqrt{3}}{4} i(|1\rangle\langle 2| - |2\rangle\langle 1| + |3\rangle\langle 4| - |4\rangle\langle 3|) \\ +\frac{1}{4} i(|2\rangle\langle 3| - |3\rangle\langle 2|) + \frac{1}{2} i(|5\rangle\langle 6| - |6\rangle\langle 5| + |7\rangle\langle 8| - |8\rangle\langle 7|) \\ -\frac{3}{4} i(|1\rangle\langle 4| - |4\rangle\langle 1|) \end{pmatrix} \cos(\omega_C t_1) \quad (3)$$

$$\sigma^S_{X,b} = 2C_Z \begin{pmatrix} \frac{\sqrt{3}}{4} (|1\rangle\langle 3| + |3\rangle\langle 1| - |2\rangle\langle 4| - |4\rangle\langle 2|) \\ +\frac{1}{4} (|2\rangle\langle 2| - |3\rangle\langle 3|) - \frac{1}{2} (|5\rangle\langle 5| - |6\rangle\langle 6| + |7\rangle\langle 7| - |8\rangle\langle 8|) \\ -\frac{3}{4} (|1\rangle\langle 1| - |4\rangle\langle 4|) \end{pmatrix} \sin(\omega_C t_1) \quad (4)$$

Here, the 'slow' $^{13}CH_3$ magnetization is temporarily converted to a mixture of 'fast' ^{1}H transitions, 'slow' ^{1}H transitions and triple-quantum transitions for one of the orthogonal components ($\sigma^S_{Y,b}$ in Eq. 3; see also Fig. 1b) and a mixture of double-quantum ^{1}H coherences and polarization states for the other component ($\sigma^S_{X,b}$ in Eq. 4; see Fig. 1b). At time-point *c*, however, the density matrix will be restored to,

$$\sigma^S_{Y,c} = -2C_Z\left(|2\rangle\langle 3| + |3\rangle\langle 2| + \frac{1}{2}|5\rangle\langle 6| + \frac{1}{2}|6\rangle\langle 5| + \frac{1}{2}|7\rangle\langle 8| + \frac{1}{2}|8\rangle\langle 7|\right)\cos(\omega_C t_1) \quad (5)$$

and

$$\sigma^S_{X,c} = -2C_Z i\left(|2\rangle\langle 3| - |3\rangle\langle 2| + \frac{1}{2}|5\rangle\langle 6| - \frac{1}{2}|6\rangle\langle 5| + \frac{1}{2}|7\rangle\langle 8| - \frac{1}{2}|8\rangle\langle 7|\right)\sin(\omega_C t_1) \quad (6)$$

Equations 5 and 6 show that the 90° ^{1}H pulse immediately preceding the time-point *c* (Fig. 1a) quantitatively restores the slowly relaxing ^{1}H magnetization (transitions shown with red arrows in Fig. 1b) leaving it in an anti-phase state with respect to ^{13}C. The last $2\tau_a$ period simply refocuses methyl ^{1}H magnetization with respect to ^{13}C before acquisition giving at point *d* (Fig. 1a),

$$\sigma^S_{Y,d} = -i\left(|2\rangle\langle 3| - |3\rangle\langle 2| + \frac{1}{2}|5\rangle\langle 6| - \frac{1}{2}|6\rangle\langle 5| + \frac{1}{2}|7\rangle\langle 8| - \frac{1}{2}|8\rangle\langle 7|\right)\cos(\omega_C t_1) \quad (7)$$

$$\sigma^S_{X,d} = -\left(|2\rangle\langle 3| + |3\rangle\langle 2| + \frac{1}{2}|5\rangle\langle 6| + \frac{1}{2}|6\rangle\langle 5| + \frac{1}{2}|7\rangle\langle 8| + \frac{1}{2}|8\rangle\langle 7|\right)\sin(\omega_C t_1) \quad (8)$$

The sum and the difference of the magnetization represented by $\sigma^S_{Y,d}$ and $\sigma^S_{X,d}$ in Eqs. 7 and 8 effectively represents a phase-modulated signal that can be acquired and processed using the standard gradient enhanced sensitivity scheme (Kay et al. 1992; Schleucher et al. 1994). Importantly, the two orthogonal pathways have different relaxation properties as between points *b* and *c* in Fig. 1a the density matrix elements given in Eqs. 3 and 4 will relax very differently. It is, therefore, critical to 'balance' the two pathways by the use of gradient coherence selection in order to avoid the generation of quadrature artifacts in the spectra.

Fast relaxation of the density matrix elements created by the application of the 90° proton pulse immediately preceding point *b* in the pulse-scheme of Fig. 1a (given by $\sigma^S_{Y,b}$ and $\sigma^S_{X,b}$ in Eqs. 3 and 4 represents the major limitation of such a PEP-HMQC scheme. Indeed, the 90° ^1H_y pulse before point *b* (partially) converts the 'slow' coherences to the 'fast' ones in one of the orthogonal pathways (Eq. 3). Since some inter-mix between the fast- and slow-relaxing parts is allowed in the scheme of Fig. 1a, it represents only a *quasi*-TROSY approach. That is why the preservation of equivalent pathways in this case is not associated with an increase in sensitivity, with the signal-to-noise values attainable using the scheme of Fig. 1a on the order of ¾ of the signal-to-noise in a regular Methyl-HMQC experiment performed in H_2O (Guo et al. 2008). Furthermore, differential relaxation of the density matrix elements in Eqs. 3 and 4 can lead to some 'leakage' of magnetization from the fast-relaxing terms present between points *b* and *c* to the slow-relaxing coherences at point *d* before direct signal acquisition. Accurate numerical simulations of this effect would require the knowledge of exact relaxation rates of all types of transitions in Eqs. 3 and 4. These relaxation rates would in turn strongly depend upon the proximity of a given methyl to other protons in the protein structure. However, approximate estimates show that such a 'fast-to-slow leakage' of magnetization is a small effect and should not exceed $\sim$10–15% of the total intensity of the 'slow' part of the signal at point *d* of the scheme (Fig. 1a).

The same analysis as above performed for the fast-relaxing orthogonal parts of the signal, σ^F_Y and σ^F_X, gives from the time-point *a* (Fig. 1a),

$$\sigma^F_{Y,a} = \sqrt{3}C_Y(|1\rangle\langle 2| + |2\rangle\langle 1| + |3\rangle\langle 4| + |4\rangle\langle 3|)\cos(\omega_C t_1) \tag{9}$$

$$\sigma^F_{X,a} = -\sqrt{3}C_X(|1\rangle\langle 2| + |2\rangle\langle 1| + |3\rangle\langle 4| + |4\rangle\langle 3|)\sin(\omega_C t_1) \tag{10}$$

to the time-point d,

$$\sigma^F_{Y,d} = -\frac{\sqrt{3}}{2}i(|1\rangle\langle 2| - |2\rangle\langle 1| + |3\rangle\langle 4| - |4\rangle\langle 3|)\cos(\omega_C t_1) \tag{11}$$

$$\sigma^F_{X,d} = \frac{\sqrt{3}}{2}(|1\rangle\langle 2| + |2\rangle\langle 1| + |3\rangle\langle 4| + |4\rangle\langle 3|)\sin(\omega_C t_1) \tag{12}$$

The fast-relaxing part of the signal is restored at point d and can be treated in the same manner as described above for its slow-relaxing counterpart. However, the density matrix elements of $\sigma^F_{X,d}$ in Eq. 12 have opposite signs compared to $\sigma^S_{X,d}$ in Eq. 8. As a result, the slow- and fast-relaxing components of the signal during t_2 evolve in the opposite senses. Therefore, the fast-relaxing part can be selected for, if necessary, simply by inversion of the sign of the gradient G6 in Fig. 1a (Guo et al. 2008).

3D NOESY pulse schemes with simultaneous detection of amide and methyl groups

Figure 2a shows a pulse scheme for a 3D SIM-^{1}H$_m$/^{1}HN-NOESY-^{13}C$_m$–^{1}H$_m$/^{15}N–^{1}HN TROSY experiment with simultaneous detection of amide and methyl groups (Guo et al. 2008) where TROSY-type magnetization transfer in $^{13}CH_3$ methyls (see Fig. 1a and discussion above) is synchronized with the ^{1}H–^{15}N amide TROSY transfer (Pervushin et al. 1997) in the implementation of Yang and Kay (1999). The use of selective proton pulses of SNEEZE variety (Nuzillard and Freeman 1994) (marked with single asterisks in Fig. 2) that selectively excite the HN-amide region of the spectra and the RE-BURP (Geen and Freeman 1991) pulse (double asterisks in Fig. 2) that excites the methyl region exclusively, preserves the 'slow' multiple-quantum coherences of $^{13}CH_3$ groups in t_2 and t_3 without disturbing the slowly relaxing component of ^{1}H–^{15}N amides (Guo et al. 2008). Simultaneous gradient selection of slowly relaxing components of ^{1}H–^{15}N and $^{13}CH_3$ signals is possible through application of a bipolar pair of gradients G4 while carbon magnetization is aligned along the z-axis. The strengths of coherence-selection gradients (G4, G5 and G8) are adjusted to simultaneously satisfy the following relationships,

$$G5/G8 = -\gamma_H/2\gamma_C \tag{13}$$

$$(G4 + G5)/G8 = -\gamma_H/2\gamma_N \tag{14}$$

where γ_i is the gyromagnetic ratio of nucleus i.

Generally, all types of inter-proton NOEs are detected in the experiment of Fig. 2a. The flow of magnetization can proceed along any one of the following pathways,

$$^{1}H_m(t_1) \xrightarrow{NOE} {}^{1}H_m \rightarrow {}^{13}C_m(t_2) \rightarrow {}^{1}H_m(t_3) \tag{I}$$

$$^{1}H_m(t_1) \xrightarrow{NOE} {}^{1}HN \rightarrow {}^{15}N(t_2) \rightarrow {}^{1}HN(t_3) \tag{II}$$

$$^{1}HN(t_1) \xrightarrow{NOE} {}^{1}HN \rightarrow {}^{15}N(t_2) \rightarrow {}^{1}HN(t_3) \tag{III}$$

$$^{1}HN(t_1) \xrightarrow{NOE} {}^{1}H_m \rightarrow {}^{13}C_m(t_2) \rightarrow {}^{1}H_m(t_3) \tag{IV}$$

As opposed to a similar study by Wagner and co-workers where all NOEs were extracted from a single time-shared experiment (Frueh et al. 2006), here we concentrate on pathways II and IV that provide (symmetric) methyl-HN and HN-methyl NOE cross-peaks. Due to a limited chemical shift dispersion of methyl ^{1}H resonances (98% of all ^{1}H$_m$ chemical shifts are clustered in the region between 0 and 1.4 ppm in MSG), it is possible to adjust the spectral width in the F_1(^{1}H$_m$) dimension of the experiment in Fig. 2a so that the overlap between methyl-methyl (pathway I), HN-HN (pathway III) and methyl-HN NOEs is minimal (SW$_{F1}$ = 5 ppm used in this work, see 'Methods'). Of note, the equilibration of water-suppression quality between the real and imaginary points in t_1 is achieved via incrementation of $\phi 1$ by 45° (Fig. 2a) (Stonehouse et al. 1994).

Figure 2b shows a pulse scheme element to be used in a 3D SIM-^{13}C$_m$/^{15}N-NOESY-^{13}C$_m$–^{1}H$_m$/^{15}N–^{1}HN TROSY experiment where all the interacting protons are labeled with the ^{15}N/^{13}C chemical shifts of attached heteronuclei. Here, methyl magnetization is preserved in a multiple-quantum Methyl-TROSY state (Tugarinov et al. 2003) in t_1 via application of selective SNEEZE pulses with excitation profiles restricted to the amide region (Fig. 2b). The phases of these selective ^{1}H pulses and the phase $\phi 4$ of the RE-BURP methyl-selective pulse are adjusted such that the sign of HN-methyl NOE cross-peaks is opposite to that of HN-HN and methyl-methyl NOEs. A phase-cycling procedure can be implemented that separates HN-methyl NOE peaks from HN-HN and methyl-methyl cross-peaks by addition/subtraction of sub-spectra (Frueh et al. 2006). As the spectrum of Fig. 2b was only occasionally used in the assignment process (see below), such a procedure has not been implemented here.

The simultaneous ^{1}H–^{15}N/$^{13}CH_3$ TROSY-type detection scheme of Guo et al. 2008, leads to average sensitivity losses of 24% and 35% in comparison with individual 2D ^{1}H–^{15}N TROSY (Yang and Kay 1999) and Methyl-HMQC (Tugarinov et al. 2003) experiments recorded on MSG in H_2O (37°C), respectively (Guo et al 2008). Using well separated diagonal and cross-peaks in the amide regions of

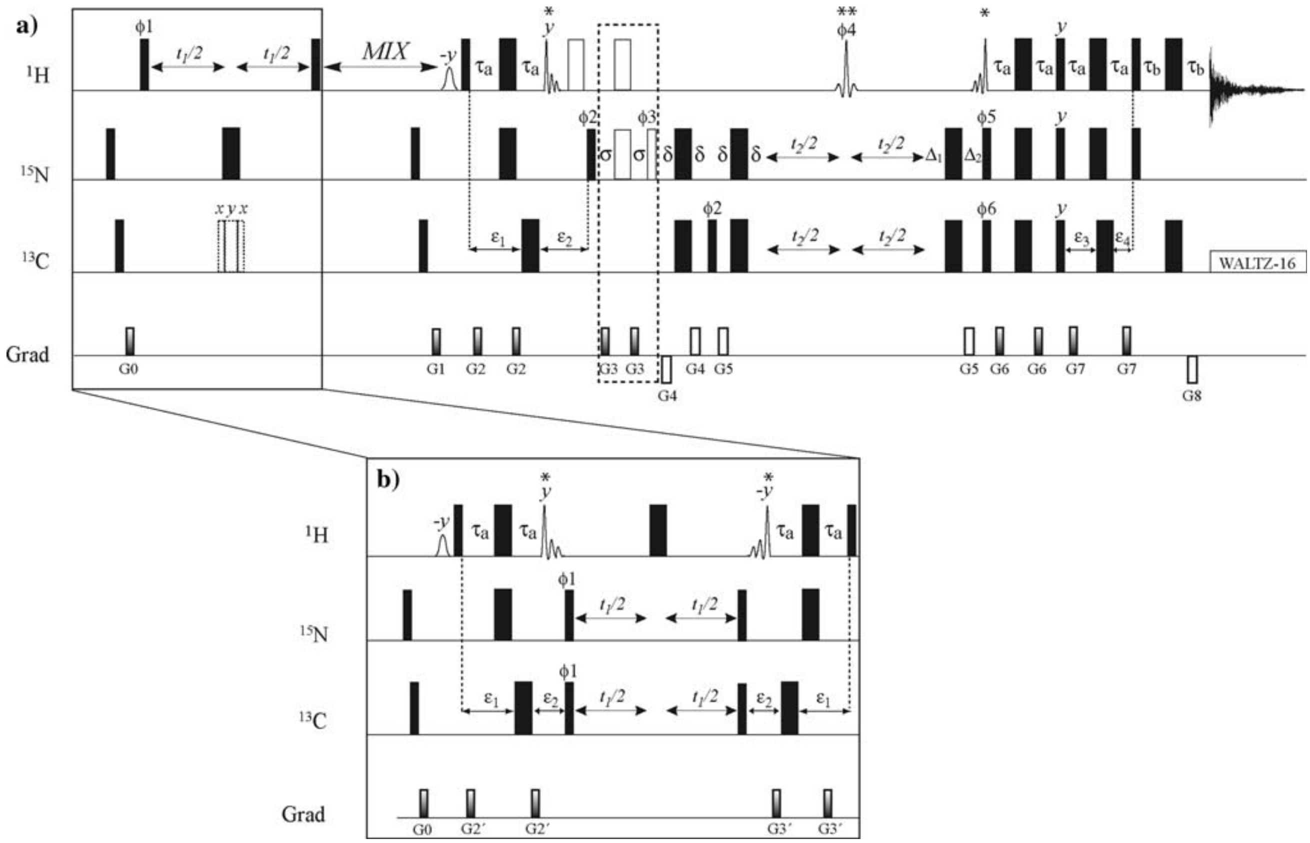

Fig. 2 Pulse schemes for the time-shared **a** 3D SIM-$^1H_m/^1$HN-NOESY-$^{13}C_m$–$^1H_m/^{15}$N–^{1}HN TROSY, and **b** 3D SIM-$^{13}C_m/^{15}$N-NOESY-$^{13}C_m$–$^1H_m/^{15}$N–^{1}HN TROSY experiments. All narrow (wide) rectangular pulses are applied with flip angles of 90(180)° along the *x*-axis unless indicated otherwise. All ^{1}H and ^{13}C rectangular pulses are applied with the highest possible power, while ^{13}C WALTZ-16 (Shaka et al. 1983) decoupling is achieved using a 2-kHz field. The ^{1}H, ^{15}N and ^{13}C carrier frequencies are positioned at 4.7, 119 and 23 ppm, respectively. Water-selective ^{1}H pulses shown with open gaussian shapes at half-height have an E-BURP-1 shape (Geen and Freeman 1991) and duration of 7 ms. ^{1}H pulses marked with asterisks are 1.25 ms time-reversed SNEEZE (phase *y*) and SNEEZE shapes (Nuzillard and Freeman 1994), respectively, (600 MHz) with the center of excitation shifted to 8 ppm via phase modulation of RF field (Boyd and Soffe 1989; Patt 1992) for excitation of amide protons and the water signal. The pulse marked with double asterisks ($\phi 4$) is a 1.25 ms RE-BURP pulse (Geen and Freeman 1991) centered at −1.1 ppm via phase modulation of RF field for selective refocusing of methyl protons. The second ^{13}C pulse in (**b**) shown with dashed lines is of a composite $90_x - 240_y - 90_x$° variety (Ernst et al. 1987). Delays are: $\tau_a = 2.3$ ms; $\tau_b = 2$ ms; $\sigma = 1.33$ ms; $\delta = 0.5$ ms; $\varepsilon_1 = 3.1$ ms; $\varepsilon_2 = 2.5$ ms; $\varepsilon_3 = 2.6$ ms; $\varepsilon_4 = 2.0$ ms. Delays Δ_i are carefully adjusted to avoid evolution of methyl ^{1}H chemical shifts before and during t_2 period: $\Delta_1 = 3\delta + \mathrm{pw_N}$; $\Delta_2 = 3\delta + \mathrm{pw_N} + \mathrm{P}_{\phi 4}$, where $\mathrm{pw_N}$ is the length of nitrogen pulse, and $\mathrm{P}_{\phi 4}$ is the length of the RE-BURP methyl-selective pulse. '*MIX*' denotes NOE mixing period. Durations and strengths of pulsed-field gradients in units of (ms; G/cm) are: G0 = (1; 15); G1 = (1.2; 15); G2′ = (0.2; 10); G3′ = (0.2; 12); G2 = (0.3; 5); G4 = (0.35; 24); G5 = (0.35; 16); G6 = (0.25; 15); G7 = (0.3; 20); G8 = (0.35; −8). Coherence-selection gradients (G4, G5 and G8) are shown with open rectangles. Phase cycle is: **a** $\phi 1 = 45°,225°$; $\phi 2 = 2(x),2(-x)$; $\phi 4 = y,-y$; $\phi 5 = \phi 6 = x$; rec. = $x,-x,-x,x$; **b** $\phi 1 = x,-x$; $\phi 2 = 2(x),2(-x)$; $\phi 4 = x,-x$; $\phi 5 = \phi 6 = x$; rec. = $x,-x,-x,x$. Quadrature detection in t_1 is achieved via States-TPPI (Marion et al. 1989). Quadrature detection in t_2 is achieved via a gradient enhanced sensitivity scheme: for each t_2 value a pair of spectra is recorded with $\phi 5$, $\phi 6 = x$; G8 and $\phi 5$, $\phi 6 = -x$; −G8 and manipulated post-acquisition (Kay et al. 1992; Schleucher et al. 1993). The phase $\phi 2$ is inverted for each t_2 point. For active suppression of the anti-^{1}H–^{15}N TROSY component (not used for MSG) the element enclosed in dashed box should be included together with the adjacent open ^{1}H π pulse. Then, G3 = (0.3; 12); $\phi 3 = 2(45°),2(225°)$, and $\phi 5$ should be incremented by 45° in order to insure the same phase for methyl and amide signals in F_2

2D $F_1(^1H_m/^{13}C_m)/F_3(^1$HN) spectra we have verified that the experiments in Figs. 2a and b suffer from similar sensitivity losses in comparison with the previously recorded ^1H_m–($^{13}C_m$)–^{15}N–^{1}HN and (^1H_m)–$^{13}C_m$–^{15}N–^{1}HN HMQC–NOESY–TROSY data sets. In particular, the SIM-$^1H_m/^1$HN-NOESY-$^{13}C_m$–$^1H_m/^{15}$N–^{1}HN TROSY experiment (Fig. 2a) proves to be on average 14% less sensitive than its ^1H_m–($^{13}C_m$)–^{15}N–^{1}HN HMQC–NOESY–TROSY counterpart, whereas the SIM-$^{13}C_m/^{15}$N-NOESY-$^{13}C_m$–$^1H_m/^{15}$N–^{1}HN TROSY experiment (Fig. 2b) features a sensitivity loss of 38% on average compared to the (^1H_m)–$^{13}C_m$–^{15}N–^{1}HN HMQC–NOESY–TROSY spectrum. However, sensitivity losses notwithstanding, the preservation of HN-methyl cross-peak symmetry in the

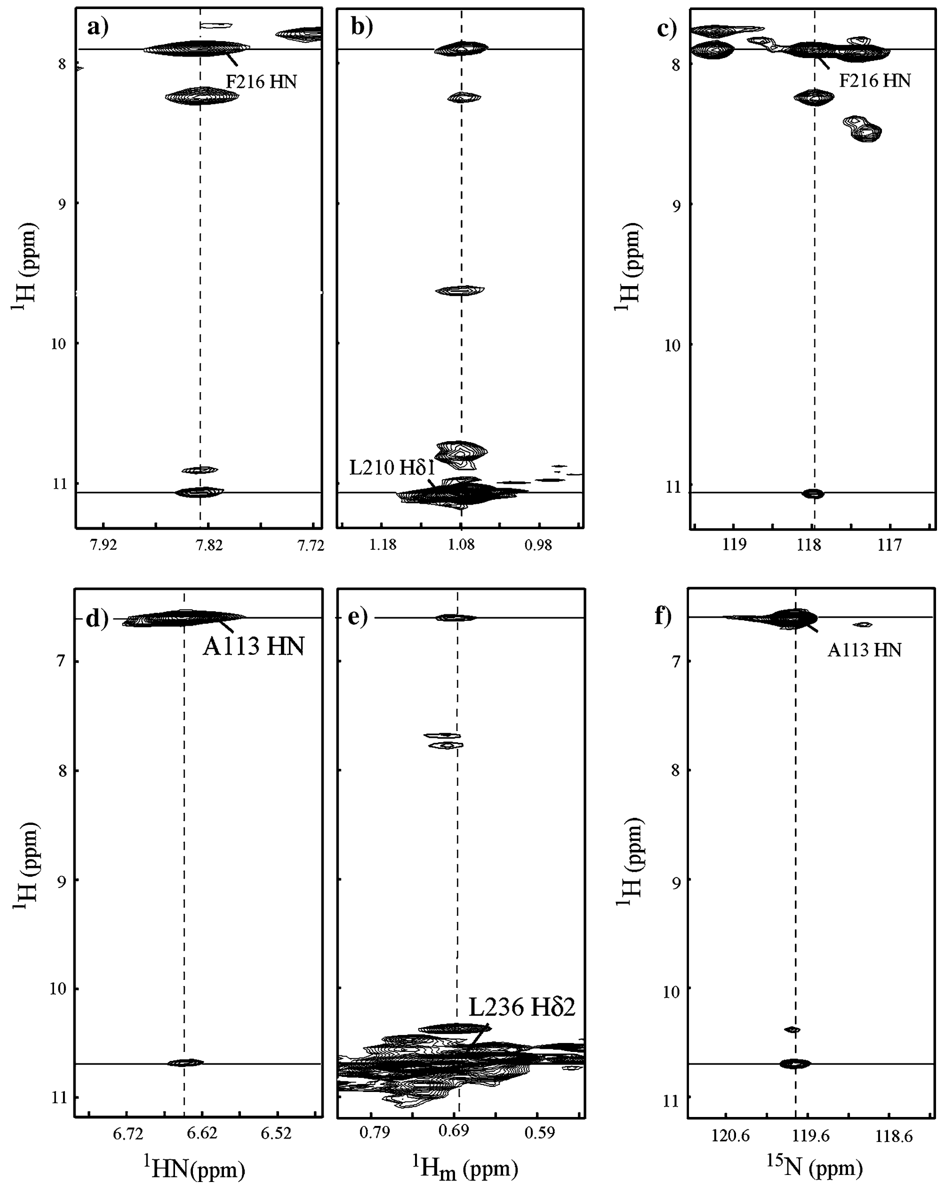

Fig. 3 Cross-peak symmetry-based assignments of long-range HN-Methyl NOEs in {U-[^{15}N,^{2}H]; Ile-[^{13}CH$_3$]; Leu,Val-[^{13}CH$_3$/^{12}CD$_3$]}-MSG (37°C, 600 MHz) using the 3D SIM-^{1}H$_m$/^{1}HN-NOESY-^{13}C$_m$–^{1}H$_m$/^{15}N–^{1}HN TROSY spectra recorded with the pulse scheme of Fig. 1a. Shown in (**a**, **b**) and (**d**, **e**) are the regions of F_1(^{1}H)/F_3(^{1}HN/^{1}H$_m$) 2D planes drawn at F_2(^{15}N/^{13}C$_m$) chemical shift of **a** F216 amide ($\Omega_N = 118$ ppm), **b** L210δ1 methyl ($\Omega_C = 28.1$ ppm) and **d** A113 amide ($\Omega_N = 119.7$ ppm), **e** L236δ2 methyl ($\Omega_C = 22.5$ ppm). Diagonal peaks are labeled with residue numbers. Shown in (**c**, **f**) are the regions of F_1(^{1}H)/F_2(^{15}N) 2D planes drawn at F_3(^{1}NH) chemical shifts of (**c**) the amide of F216 ($\Omega_{HN} = 7.83$ ppm), and (**d**) the amide of A113 ($\Omega_{HN} = 6.65$ ppm). Such 2D cross-sections through the 3D spectrum are useful in locating the symmetrical NOE cross-peaks in the 3D data matrix (see text). Note that methyl diagonal peaks are double-aliased in the F_1(^{1}H) dimension and their true chemical shifts are obtained by subtraction of $2 \times SW_{F1} = 10$ ppm from the observed values (see 'Methods')

^{1}H–^{15}N/^{13}CH$_3$ time-shared data significantly simplifies the process of NOE assignments in the overcrowded spectra of large protein molecules.

Despite lower sensitivity of the experiments described here, 333(127) HN-methyl NOEs(long-range HN-methyl NOEs, $|i - j| > 3$) could be identified and assigned in the time-shared data sets of Fig. 2 recorded at 600 MHz on a room-temperature probe compared to 357(142) HN-Methyl NOEs available from 3D ^{1}H$_m$–(^{13}C$_m$)–^{15}N–^{1}HN and (^{1}H$_m$)–^{13}C$_m$–^{15}N–^{1}HN HMQC–NOESY–TROSY data sets acquired previously by Tugarinov et al. 2005 at the same spectrometer field using a cryogenically cooled probe. Below, we illustrate with a couple of examples that cross-peak symmetry in the simultaneous ^{1}H–^{15}N/^{13}CH$_3$ time-shared NOESY data is of great aid for unambiguous NOE assignments.

Symmetry-based identification of HN-methyl NOEs in MSG

Both the 3D ^{1}H$_m$–(^{13}C$_m$)–^{15}N–^{1}HN and (^{1}H$_m$)–^{13}C$_m$–^{15}N–^{1}HN HMQC–NOESY–TROSY experiments used for assignments of HN-methyl NOEs in MSG (Tugarinov et al. 2005) lack cross-peak symmetry. When several NOE cross-peaks originate from a single amide, these spectra do not contain sufficient information on the ^{1}H–^{13}C connectivity. For example, in the case when three cross-peaks originate from a single amide in each of the two spectra, there are nine possibilities for the ^{1}H–^{13}C connectivity. The number of possibilities can be reduced by inspection of the 2D ^{1}H–^{13}C HMQC spectrum for the presence/absence of peaks at a given pair of ^{1}H,^{13}C chemical shifts. However, 2D methyl ^{1}H/^{13}C correlation maps of such large

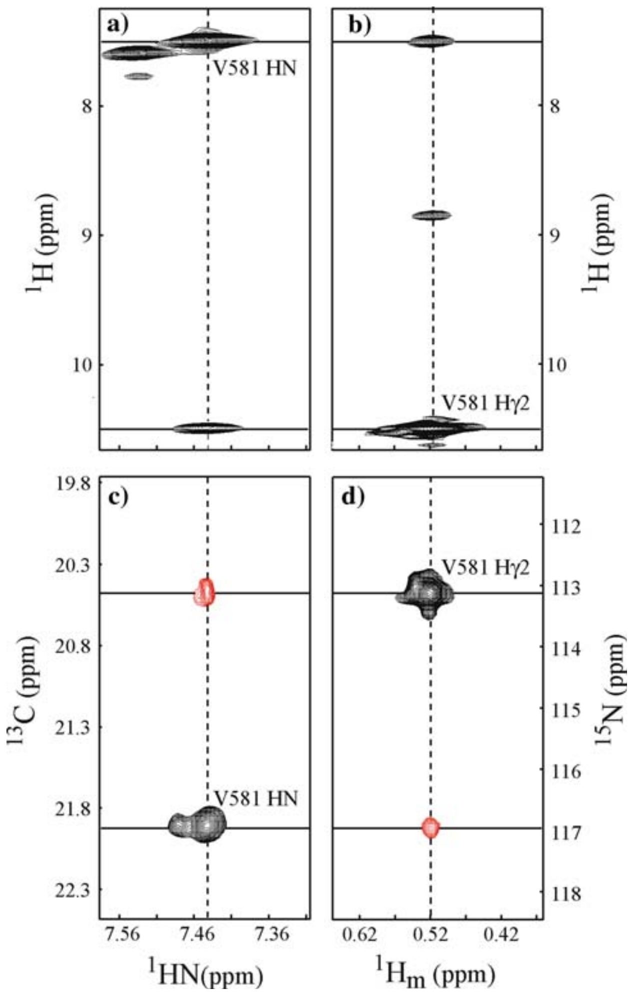

Fig. 4 Symmetry-based assignment of intra-residual HN-Methyl NOEs in {U-[^{15}N,^{2}H]; Ile-[^{13}CH$_3$]; Leu,Val-[^{13}CH$_3$/^{12}CD$_3$]}-MSG (37°C, 600 MHz) using both (**a**, **b**) 3D SIM-^{1}H$_m$/^{1}HN-NOESY-^{13}C$_m$–^{1}H$_m$/^{15}N–^{1}HN TROSY and (**c**, **d**) SIM-^{13}C$_m$/^{15}N-NOESY-^{13}C$_m$–^{1}H$_m$/^{15}N–^{1}HN TROSY time-shared experiments recorded with the pulse-schemes shown in Figs. 2a and b, respectively. Shown in (**a**, **b**) are the regions of F_1(^{1}H)/F_3(^{1}HN/^{1}H$_m$) 2D planes drawn at F_2(^{15}N/^{13}C$_m$) chemical shift of (**a**) the amide of V581 ($\Omega_N = 116.9$ ppm), (**b**) V581γ2 methyl ($\Omega_C = 20.3$ ppm). Panels (**c**, **d**) show the cross-peak symmetry obtained in the SIM-^{13}C$_m$/^{15}N-NOESY-^{13}C$_m$–^{1}H$_m$/^{15}N–^{1}HN TROSY experiment. Negative peaks are shown with red contours; diagonal peaks are labeled with residue numbers. The spectra in panels (**c**) and (**d**) are labeled with ^{13}C and ^{15}N chemical shifts along the F_1 dimension, respectively, so that only (negative) HN-methyl NOE cross-peaks are characterized by correct frequency labeling (in ppm) facilitating the identification of ^{15}N/^{13}C chemical shifts of destination nuclei

monomeric proteins as MSG tend to be overlapped frequently precluding unambiguous assignments. Furthermore, the problems of NOE assignments and establishing the correct ^{1}H-^{13}C connectivity are often aggravated by overlap of resonances in either ^{1}H$_m$–^{13}C$_m$–^{15}N–^{1}HN HMQC–NOESY–TROSY or (^{1}H$_m$)–^{13}C$_m$–^{15}N–^{1}HN HMQC–NOESY–TROSY experiment or both. Such ambiguities frequently make NOE assignments unreliable. Obviously, the HN-methyl NOE symmetry may be restored by recording additional 3D ^{1}HN–(^{15}N)–^{13}C$_m$–^{1}H$_m$ and (^{1}HN)–^{15}N–^{13}C$_m$–^{1}H$_m$ HSQC–NOESY–HMQC data sets at the expense of approximately twice more instrument time. Instead, the cross-peak symmetry is conveniently restored in the time-shared NOESY datasets recorded with simultaneous amide-methyl detection schemes of Fig. 2.

Figure 3a, b, d and e shows F_1(^{1}H)/F_3(^{1}HN/^{1}H$_m$) 2D planes of the 3D SIM-^{1}H$_m$/^{1}HN-NOESY-^{13}C$_m$–^{1}H$_m$/^{15}N–^{1}HN TROSY spectrum of {U-[^{15}N,^{2}H]; Ile-[^{13}CH$_3$]; Leu,Val-[^{13}CH$_3$/^{12}CD$_3$]}-MSG drawn at F_2(^{15}N/^{13}C$_m$) chemical shifts of F216 amide (3a), L210δ1 methyl (3b), A113 amide (3d) and L236δ2 methyl (3e). Symmetrical cross-peaks identify NOE interactions between the amide of F216 and L210δ1 methyl (3a and 3b) and between the amide of A113 and L236δ2 methyl (3d and 3e). The distances between the geometric center of L210δ1(L236δ2) methyl protons and the amide proton of F216(A113) measured from the X-ray structure of MSG (Howard et al. 2000) correspond to 3.1 Å(4.1 Å). Clearly, symmetry is of great help for NOE cross-peak assignments. Symmetric peaks can be located in the 3D data matrix by inspection of F_1(^{1}H)/F_2(^{15}N) 2D planes drawn at F_3(^{1}NH) chemical shift equal to the F_1(^{1}H) chemical shift of the cross-peak of interest as it is illustrated in Fig. 4c for the L210δ1–F216HN interacting pair and Fig. 4f for the L236δ2–A113HN pair. Note that in F_1(^{1}H), ^{1}HN chemical shifts will differ from their values in F_3(^{1}HN) by $-^1J_{NH}/2$, where $^1J_{NH}$ is a one-bond ^{15}N–^{1}H coupling constant (+0.08 ppm at 600 MHz; $^1J_{NH} < 0$), by virtue of the non-TROSY-type acquisition in the F_1(^{1}H) dimension and the TROSY-type acquisition in F_3(^{1}HN) (see Fig. 2a).

The vast majority of NOE cross-peaks in MSG can be assigned using the symmetry properties of a single time-shared SIM-^{1}H$_m$/^{1}HN-NOESY-^{13}C$_m$–^{1}H$_m$/^{15}N–^{1}HN TROSY experiment. In some cases (and especially for intra-residual NOE interactions), it may be helpful to refer to the 3D SIM-^{13}C$_m$/^{15}N-NOESY-^{13}C$_m$–^{1}H$_m$/^{15}N–^{1}HN TROSY data (experiment of Fig. 2b). This latter experiment is, however, less sensitive than its proton-based counterpart and is a source of primarily intra-residual NOE interactions. Figures 4a–d show how NOE assignments can be obtained using both experiments for the intra-residual interaction between the amide of V581 and its γ2 methyl group. The signs of HN-methyl cross-peaks (shown with red contours in Fig 4c and d) are opposite to the signs of all the other cross- and diagonal peaks in this spectrum. Note that ^{15}N chemical shifts of NOE cross-peaks in the F_1 dimension, will differ from their values in F_2(^{15}N) by $^1J_{NH}/2$ (−0.8 ppm at 600 MHz), as a result of the non-TROSY type of acquisition in F_1(^{15}N) and the TROSY-type acquisition in F_2(^{15}N).

In summary, we have presented a pair of NOESY experiments with simultaneous TROSY-based detection of amide and methyl groups for identification of HN-methyl NOE interactions in high-molecular-weight proteins. The symmetry of cross-peaks in the resulting data sets is of great aid for assignments of HN-methyl NOEs in large and complex protein structures. The pulse schemes are designed to preserve the slowly decaying components of both ^{1}H–^{15}N and methyl $^{13}CH_3$ spin-systems in the course of indirect evolution (t_2) and acquisition period (t_3) of 3D NOESY experiments. More than 300 HN-methyl NOEs and more than 100 long-range ($|i - j| > 3$) HN-methyl interactions could be identified and assigned in {U-[^{15}N,^{2}H]; Ileδ1-[$^{13}CH_3$]; Leu,Val-[$^{13}CH_3$,$^{12}CD_3$]}-labeled MSG from a single $^{15}N/^{13}C$ time-shared 3D NOESY data set acquired using simultaneous amide-methyl detection scheme providing important distance restraints for the derivation of backbone global fold. We hope that the experiments described here will serve as a valuable addition to the array of NMR techniques suitable for the studies of large proteins.

Acknowledgment This work was supported in part by the Nano-Biotechnology Award to V.T. The authors thank Prof. David Fushman (University of Maryland) for stimulating discussions and Dr. Devon Sheppard (University of Maryland) for carefully reading the manuscript.

References

Bax A, Griffey RH, Hawkings BL (1983) Correlation of proton and nitrogen-15 chemical shifts by multiple quantum NMR. J Magn Reson 55:301–315

Boelens R, Burgering M, Fogh RH, Kaptein R (1994) Time-saving methods for heteronuclear multidimensional NMR of (^{13}C, ^{15}N) doubly labeled proteins. J Biomol NMR 4:201–213

Boyd J, Soffe N (1989) Selective excitation by pulse shaping combined with phase modulation. J Magn Reson 85:406–413

Delaglio F, Grzesiek S, Vuister GW, Zhu G, Pfeifer J, Bax A (1995) NMRPipe: a multidimensional spectral processing system based on UNIX pipes. J Biomol NMR 6:277–293

Ernst RR, Bodenhausen G, Wokaun A (1987) Principles of nuclear magnetic resonance in one and two dimensions. Oxford University Press, Oxford

Farmer BTII (1991) Simultaneous [^{13}C, ^{15}N]-HMQC, a pseudo-triple-resonance experiment. J Magn Reson 93:635–641

Farmer BTII, Mueller L (1994) Simultaneous acquisition of [^{13}C, ^{15}N]- and [^{15}N, ^{15}N]-separated 4D gradient-enhanced NOESY spectra in proteins. J Biomol NMR 4:673–687

Frueh D, Vosburg D, Walsh C, Wagner G (2006) Determination of all nOes in ^{1}H-^{13}C-Me-ILV-U-^{2}H-^{15}N proteins with two time-shared experiments. J Biomol NMR 34:31–40

Gardner KH, Kay LE (1997) Production and incorporation of ^{15}N, ^{13}C, ^{2}H (^{1}H-δ1 methyl) isoleucine into proteins for multidimensional NMR studies. J Am Chem Soc 119:7599–7600

Gardner KH, Rosen MK, Kay LE (1997) Global folds of highly deuterated, methyl protonated proteins by multidimensional NMR. Biochemistry 36:1389–1401

Gardner KH, Zhang X, Gehring K, Kay LE (1998) Solution NMR studies of a 42-kDa *E. coli* maltose binding protein/β cyclodextrin complex: chemical shift assignments and analysis. J Am Chem Soc 120:11738–11748

Geen H, Freeman R (1991) Band-selective radiofrequency pulses. J Magn Reson 93:93–141

Goto NK, Gardner KH, Mueller GA, Willis RC, Kay LE (1999) A robust and cost-effective method for the production of Val, Leu, Ile (δ1) methyl-protonated 15N-, 13C-, 2H-labeled proteins. J Biomol NMR 13:369–374

Guo C, Zhang D, Tugarinov V (2008) An NMR experiment for simultaneous TROSY-based detection of amide and methyl groups in large proteins. J Am Chem Soc 130:10872–10873

Howard BR, Endrizzi JA, Remington SJ (2000) Crystal structure of *Escherichia coli* malate synthase G complexed with magnesium and glyoxylate at 2.0 A resolution: mechanistic implications. Biochemistry 39:3156–3168

Johnson BA, Blevins RA (1994) NMRView: a computer program for the visualization and analysis of NMR data. J Biomol NMR 4:603–614

Kay LE, Prestegard JH (1987) Methyl group dynamics from relaxation of double quantum filtered NMR signals. Application to deoxycholate. J Am Chem Soc 109:3829–3835

Kay LE, Keifer P, Saarinen T (1992) Pure absorption gradient enhanced heteronuclear single quantum correlation spectroscopy with improved sensitivity. J Am Chem Soc 114:10663–10665

Marion D, Ikura M, Tschudin R, Bax A (1989) Rapid recording of 2D NMR spectra without phase cycling. Application to the study of hydrogen exchange in proteins. J Magn Reson 85:393–399

Mueller L (1979) Sensitivity enhanced detection of weak nuclei using heteronuclear multiple quantum coherence. J Am Chem Soc 101:4481–4484

Muhandiram DR, Xu GY, Kay LE (1993) An enhanced-sensitivity pure absorption gradient 4D ^{15}N, ^{13}C-edited NOESY experiment. J Biomol NMR 3:463–470

Nuzillard JM, Freeman R (1994) Oversampling in two-dimensional NMR. J Magn Reson A 110:252–258

Ollerenshaw JE, Tugarinov V, Kay LE (2003) Methyl TROSY: explanation and experimental verification. Magn Reson Chem 41:843–852

Palmer AG, Cavanagh J, Wright PE, Rance M (1991) Sensitivity improvement in proton-detected two-dimensional heteronuclear correlation NMR spectroscopy. J Magn Reson 93:151–170

Pascal S, Muhandiram DR, Yamazaki T, Forman-Kay JD, Kay LE (1994) Simultaneous acquisition of ^{15}N and ^{13}C edited NOE spectra of proteins dissolved in H_2O. J Magn Reson B 103: 197–201

Patt SL (1992) Single- and multiple-frequency-shifted laminar pulses. J Magn Reson 96:94–102

Pervushin K, Riek R, Wider G, Wüthrich K (1997) Attenuated T_2 relaxation by mutual cancellation of dipole–dipole coupling and chemical shift anisotropy indicates an avenue to NMR structures of very large biological macromolecules in solution. Proc Natl Acad Sci USA 94:12366–12371

Rosen MK, Gardner KH, Willis RC, Parris WE, Pawson T, Kay LE (1996) Selective methyl group protonation of perdeuterated proteins. J Mol Biol 263:627–636

Sattler M, Maurer M, Schleucher J, Griesinger C (1995) A simultaneous ^{15}N, ^{1}H- and ^{13}C, ^{1}H-HSQC with sensitivity enhancement and a heteronuclear gradient echo. J Biomol NMR 5:97–102

Schleucher J, Sattler M, Griesinger C (1993) Coherence selection by gradients without signal attenuation: application to the three-dimensional HNCO experiment. Angew Chem Int Ed Engl 32:1489–1491

Schleucher J, Schwendinger M, Sattler M, Schmidt P, Schedletzky O, Glaser SJ, Sorensen OW, Griesinger C (1994) A general enhancement scheme in heteronuclear multidimensional NMR employing pulsed field gradients. J Biomol NMR 4:301–306

Shaka AJ, Keeler J, Frenkiel T, Freeman R (1983) An improved sequence for broadband decoupling: WALTZ-16. J Magn Reson 52:335–338

Sorensen OW (1990) Aspects and prospects of multidimensional time-domain spectroscopy. J Magn Reson 89:210–216

Stonehouse J, Shaw GL, Keeler J, Laue ED (1994) Minimising sensitivity losses in gradient selected 15N–1H HSQC spectra of proteins. J Magn Reson A 107:178–184

Tugarinov V, Kay LE (2004) An isotope labeling strategy for methyl TROSY spectroscopy. J Biomol NMR 28:165–172

Tugarinov V, Kay LE (2005) Methyl groups as probes of structure and dynamics in NMR studies of high-molecular-weight proteins. Chembiochem 6:1567–1577

Tugarinov V, Muhandiram R, Ayed A, Kay LE (2002) Four-dimensional NMR spectroscopy of a 723-residue protein: chemical shift assignments and secondary structure of malate synthase G. J Am Chem Soc 124:10025–10035

Tugarinov V, Hwang PM, Ollerenshaw JE, Kay LE (2003) Cross-correlated relaxation enhanced 1H–13C NMR spectroscopy of methyl groups in very high molecular weight proteins and protein complexes. J Am Chem Soc 125:10420–10428

Tugarinov V, Choy WY, Orekhov VY, Kay LE (2005) Solution NMR-derived global fold of a monomeric 82-kDa enzyme. Proc Natl Acad Sci USA 102:622–627

Uhrín D, Bramham J, Winder SJ, Barlow P (2000) Simultaneous CT-13C and VT-15N chemical shift labeling: application to 3D NOESY-CH3-NH and 3D 13C, 15N-HSQC-NOESY-CH3-NH. J Biomol NMR 18:253–259

Würtz P, Aitio O, Hellman M, Permi P (2007) Simultaneous detection of amide and methyl correlations using a time shared NMR experiment: application to binding epitope mapping. J Biomol NMR 39:97–105

Wüthrich K (1986) NMR of proteins and nucleic acids. Wiley, New York

Xia Y, Yee A, Arrowsmith CH, Gao X (2003) ^{1}H(C) and ^{1}H(N) total NOE correlations in a single 3D NMR experiment. ^{15}N and ^{13}C time-sharing in t_1 and t_2 dimensions for simultaneous data acquisition. J Biomol NMR 27:193–203

Xu Y, Long D, Yang D (2007) Rapid data collection for protein structure determination by NMR spectroscopy. J Am Chem Soc 129:7722–7723

Yang D, Kay LE (1999) Improved ^{1}HN-detected triple resonance TROSY-based experiments. J Biomol NMR 13:3–10